Magneli-phase titanium suboxide nanocrystals as highly active catalysts for selective acetalization of furfural

Masanori Nagao,[a] Sayaka Misu,[a] Jun Hirayama,[a] Ryoichi Otomo,[b,*] Yuichi Kamiya[b,*]

[a] *Graduate School of Environmental Science, Hokkaido University, Kita 10 Nishi 5, Sapporo 060-0810, Japan.*

[b] *Faculty of Environmental Earth Science, Hokkaido University, Kita 10 Nishi 5, Sapporo 060-0810, Japan.*

**Corresponding authors*

Dr. Ryoichi Otomo

Tel: +81-11-706-2259, E-mail: otomo@ees.hokudai.ac.jp

Prof. Yuichi Kamiya

Tel: +81-11-706-2217, E-mail: kamiya@ees.hokudai.ac.jp

Keywords:

Titanium suboxide; Magneli-phase; Ti_2O_3; Ti_4O_7; Furfural; Acetalization; Black titania

Abstract

Alongside TiO_2, Magneli-phase titanium suboxide having the composition of Ti_nO_{2n-1} is a kind of attractive functional materials composed of titanium. However, there still remain problems to be overcome in the synthesis of titanium suboxide; the existing synthesis methods require high temperature typically over 1000 °C and/or post-synthesis purification. This study presents a novel approach to synthesis of titanium suboxide nanoparticles through solid-phase reaction of TiO_2 with TiH_2. Crystal phases of titanium suboxide were easily controlled by changing TiO_2/TiH_2 molar ratios in a TiO_2-TiH_2 mixed precursor and a series of titanium suboxide nanoparticles including Ti_2O_3, Ti_3O_5, Ti_4O_7 and Ti_8O_{15} were successfully obtained. The reaction of TiO_2 with TiH_2 proceeded at relatively low temperature due to high reactivity of TiH_2, giving titanium suboxide nanoparticles without any post-synthesis purification. Ti_2O_3 nanoparticles and TiO_2 were applied as solid acid catalysts for reaction of furfural with 2-propanol. Ti_2O_3 showed high catalytic activity and high selectivity for acetalization of furfural, while TiO_2 showed only poor activity for transfer hydrogenation of furfural. The difference in catalytic properties is discussed in terms of the acid properties of Ti_2O_3 and TiO_2.

Introduction

Titanium is ranked in the tenth element of Clarke number and is the second most abundant transition metal next to iron.[1] For making good use of limited natural resources, it is desirable to develop diverse functional materials from abundant and readily available elements like titanium. Because the most stable valence of titanium is Ti^{4+}, TiO_2 is a typical titanium oxide and has a wide range of practical applications. Meanwhile, titanium can take valence states less than Ti^{3+} and in fact, various titanium oxides containing the low-valence titanium are known.[2,3] There are two classes of low-valence titanium oxides. One is a set of titanium oxides so called “partially-reduced TiO_2”, which have nonstoichiometric compositions holding Ti^{3+} and oxygen vacancy as defects in TiO_2 crystal.[2] The other is called “Magneli-phase titanium suboxide”, which is hereafter simply called as “titanium suboxide”. Titanium suboxides have specific crystal structures different from TiO_2 depending on their stoichiometric compositions (Ti_nO_{2n-1}, $n \geq 1$).[4]

It is well known that titanium suboxides show unique electrical and optical properties, which TiO_2 does not show, serving as precursors for solar cells and electrodes.[3] Nevertheless, practical applications of titanium suboxides are very few because of complexity and difficulty in the existing synthesis methods for titanium suboxides. Conventionally, titanium suboxides have been synthesized by the reduction of TiO_2 with reductants such as gaseous compounds[5-17], carbonaceous materials[18-26] and metals with high oxygen affinity[27-30] at typically 1000 °C or higher. However, such high temperature conditions inevitably cause particle growth. Consequently, resulting titanium suboxides have extremely large particles with low surface area, which limits the scope of their

applications especially for those involving chemical reaction on their surfaces such as catalysts and electrodes. It can be expected that titanium suboxide nanoparticles with enhanced surface area could make great progress in their existing applications and open new prospects of their novel use.

In recent years, a couple of methods have been developed for the synthesis of titanium suboxide nanoparticles by using metals[31], metal hydrides,[32-37] and organic polymers[38-41] as reductants for TiO_2. Tominaka et al. developed a synthesis method using CaH_2 as a reductant[32]; Ti_2O_3 nanoparticles with the size of 50 nm or less were successfully obtained by heating TiO_2-CaH_2 mixture at 350 °C for 15 days. Kageyama et al. utilized metallic Zr as an oxygen getter for synthesizing a series of macroporous titanium suboxide monoliths[30]. However, the recent excellent methods still have a problem related to the use of elements other than titanium. Metal oxides or carbonaceous compounds always coexist in the solid products as impurities and thus, burdensome post-synthesis purification to remove them are absolutely necessary to obtain pure titanium suboxides. Moreover, to our best knowledge, there are only few synthesis methods that can easily control a crystal phase of titanium suboxide at will.

While applications of titanium suboxides to solar cells and electrodes have been investigated,[3] there is no report on application of titanium suboxides as catalysts, though they are supposed to have unique catalytic functions owing to low valence titanium. In addition, quantitative understanding of catalytic properties of titanium suboxides, which have the stoichiometric compositions, could give a helpful knowledge to clarify the complex relationship between catalytic properties and surface structures such as Ti^{3+} and/or acid-base properties of partially-reduced TiO_2,

while various chemical reactions are promoted over them, it is not still clearly understood.[42-49]

Furfural is one of the important chemicals available from carbohydrates through degradation of pentosan and dehydration of pentoses such as xylose.[50] Furfural is a platform material for the production of value-added chemicals from biomass.[50-52] An example of its functional derivatives is a series of furfural acetal, which can be applied in pharmaceutical, surfactant, and flagrance industries and also can serve as versatile intermediates in organic synthesis.[53-57] Of various types of solid acid catalysts tested so far, zeolites showed high catalytic activity and high selectivity in the acetalization of furfurals.[54,55] Another important example of furfural derivative is furfuryl alcohol, which is a precursor for furanic resins, fuel additives, and so on.[51,52,58-61] Furfuryl alcohol can be produced by transfer hydrogenation of furfural under mild conditions in the presence of Lewis acids.[58-63] However, in some cases, the acetalization and transfer hydrogenation of furfural simultaneously occur, decreasing the selectivity to a desired product.[58,59,61] Thus, the selective synthesis of furfural acetal and furfuryl alcohol is still a challenging issue.

In the present study, we propose a novel method using TiH_2 as a reductant for TiO_2 to readily synthesize titanium suboxide nanoparticles with controlled crystal phases and stoichiometric compositions. Ti_2O_3 nanoparticles synthesized in this way showed high catalytic activity and high selectivity for acetalization of furfural due to its high surface area and unique acid properties, while TiO_2 promoted only transfer hydrogenation of furfural.

Experimental

Synthesis of titanium suboxides

Titanium suboxides were synthesized by solid-phase reaction of commercial rutile TiO_2 (STR-100N, Sakai Chemical Industry) with TiH_2 (99% metals basis, Alfa Aesar). TiO_2 and TiH_2 were ground together for 30 min using a mortar with a pestle to obtain a homogeneously mixed precursor. The precursor was transferred to a quartz tube connected to a vacuum line and heated *in vacuo* for predetermined time by an electronic furnace (Figure S1). After the temperature was decreased to ambient temperature *in vacuo*, the product powder was taken out. Syntheses using TiH_2 were done with TiO_2/TiH_2 molar ratio, temperature, and synthesis time varied. A commercial Ti_2O_3 was purchased from Kojundo Chemical Laboratory, Japan and denoted as Ti_2O_3-com.

Characterization

XRD patterns of samples were collected on a Rigaku MiniFlex diffractometer with Cu Kα radiation (λ = 0.154 nm) at a step width of 0.02°. Morphology of sample particles was observed by a field-emission scanning electron microscope (SEM) using a HITACHI S-4800 at acceleration voltage of 5 kV. Observation with a transmission electron microscope (TEM) was conducted using a JEOL JEM-2100F with an acceleration voltage of 200 kV. Specific surface area was calculated by the BET method applied for a nitrogen adsorption isotherm measured on a MicrotracBEL, BELSORP-mini analyzer at liquid nitrogen temperature. Samples were pretreated at 300 °C for 1 h in N_2 flow. X-ray photoelectron spectroscopy (XPS) measurements were performed using a JEOL

JPC-9010MC X-ray photoelectron spectrometer with Mg Kα X-ray at 1253.6 eV as the excitation source. A powder sample (50 mg) was pelletized to a disk, and it was pretreated overnight under vacuum. C 1s peak (284.7 eV) derived from carbon tape was used for the charge correction.

Acid properties of the samples were examined by temperature-programmed desorption of ammonia (NH_3-TPD) using a BEL-TPD analyzer (MicrotracBEL) equipped with a quadrupole mass spectrometer ANELVA, M-QA100F. A powder sample (100 mg) was pretreated at 50 °C for 1 h in He flow (20 mL min^{-1}). After the pretreatment, the sample was exposed to NH_3 (27 kPa) for 10 min. The sample was purged with He flow (20 mL min^{-1}) at the same temperature for 0.5 h to remove physisorbed NH_3. A TPD profile was obtained by increasing the temperature of the sample from 50 to 750 °C at the rate of 10 °C min^{-1} in He flow (20 mL min^{-1}) and concentration of NH_3 (m/z = 16) in the effluent gas was monitored by the quadrupole mass spectrometer. Thermogravimetric (TG) analyses of titanium suboxide samples were operated in air flow using a differential thermogravimetric analyzer (Rigaku, Thermo Plus TG8120). A sample (10 mg) was heated from ambient temperature to 1000 °C at a rate of 10 °C min^{-1}. During the measurement, the sample gained weight due to oxidation and finally it was completely oxidized to form TiO_2. From the amount of weight gain (oxygen uptake), the average valence of titanium for a sample was calculated according to an equation (1),

$$\mathrm{Ti_{total}} = \frac{2 \times \left\{2 \times {W_f}/{79.87} - {(W_f - W_i)}/{16.00}\right\}}{{W_i}/{79.87}} \quad (1)$$

Where Ti_{total} is the average valence of total titanium mainly in the bulk, and W_i and W_f are the weight of sample before and after TG analysis, respectively.

Catalytic reaction of furfural with 2-propanol

Catalytic properties of Ti_2O_3 and TiO_2 were examined in reaction of furfural with 2-propanol (Scheme 1). A powder catalyst (25 mg) was added to 2.5 mL of 2-propanol solution of furfural (0.2 M) in a test tube and the suspension was heated at 90 °C for 2 h with stirring. The reaction was quenched by cooling the test tube in an ice bath and the suspension was centrifuged. The supernatant solution was analyzed on a GC-FID using SHIMADZU GC-2010 chromatograph equipped with a capillary column (Agilent J&W, DB-1). The amount of furfural and products in the solution was calculated according to the calibration curves. To compare catalytic properties with Ti_2O_3 and TiO_2, commercially available zeolite beta (CP-811C-300, Zeolyst) and ZrO_2 (RC-100, Daiichi Kigenso Kagaku Kogyo) were used as catalysts.

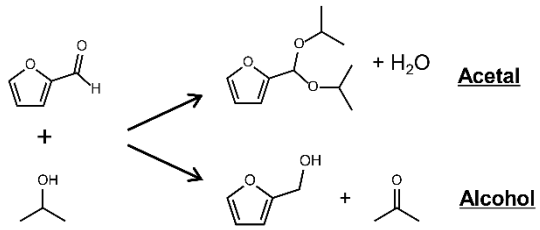

Scheme 1 Reaction pathways for acetalization and transfer hydrogenation of furfural with 2-propanol.

Results and discussion

Synthesis of Ti_2O_3 nanoparticles

First, titanium suboxide samples were synthesized by heating the precursors with

TiO_2/TiH_2 = 1, 2 and 3 at 700 °C for 72 h (Figure 1a). For all the products, the main crystal phase was rhombohedral Ti_2O_3 (JCPDS#43-1033) regardless of the TiO_2/TiH_2 ratio. Nearly single phase Ti_2O_3 was obtained from the precursor with TiO_2/TiH_2 = 2, while other crystalline phases such as Ti_4O_7, Ti_3O_5, TiO, and metallic Ti coexisted in the products for TiO_2/TiH_2 = 1 and 3.

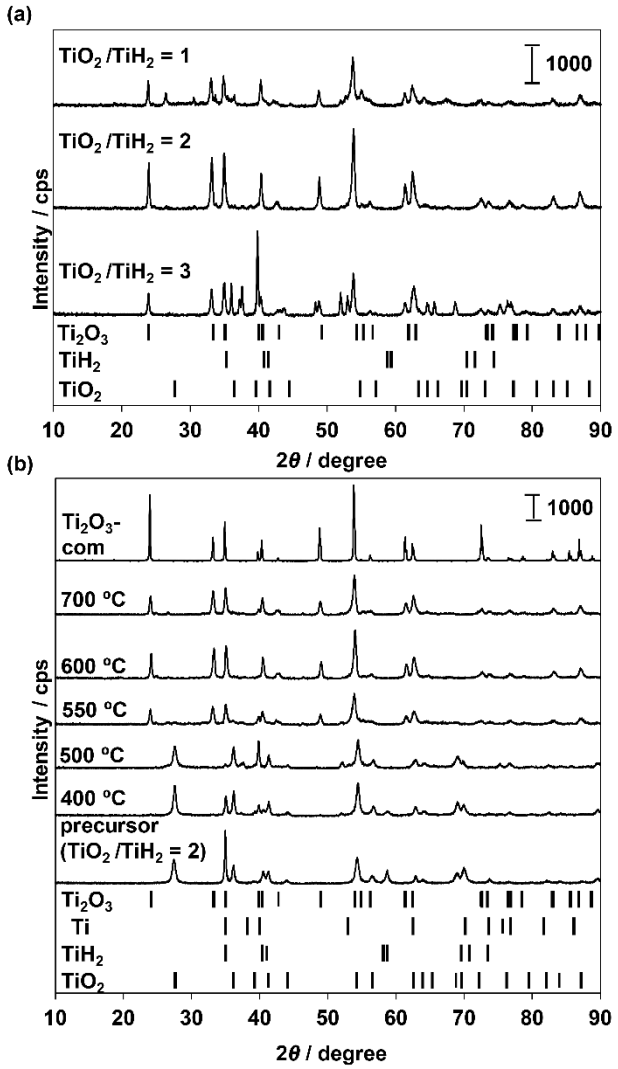

Figure 1. XRD patterns of titanium suboxides synthesized (a) by heating precursors with different TiO_2 /TiH_2 ratios at 700 °C for 72 h and (b) by heating the precursor with TiO_2 /TiH_2 = 2 at different temperatures for 24 h (exceptionally for 30 h at 550 °C).

Next, influence of the temperature was investigated using the precursor with TiO_2/TiH_2 = 2 (Figure 1b). Upon heating at 400 °C, intensities of the diffraction lines for TiH_2 significantly decreased. The diffraction pattern of TiH_2 disappeared at 500 °C and instead a diffraction pattern assignable to metallic Ti appeared. TiO_2 still remained in the product at 500 °C with the diffraction intensities comparable to those for the precursor, but disappeared at 550 °C and concurrently, Ti_2O_3 was formed as a dominant product. Namely, Ti_2O_3 was successfully obtained even at 550 °C by the present method using TiH_2. As the temperature was further increased, the diffraction lines of Ti_2O_3 became sharp due to crystallite growth and no other crystalline phase appeared. The samples synthesized at 550, 600 and 700 °C in Figure 1b are denoted as Ti_2O_3-TH550, Ti_2O_3-TH600, and Ti_2O_3-TH700, respectively.

The changes in crystalline structures shown in Figure 1 indicated that TiH_2 was transformed into metallic Ti with evolution of H_2 at ~500 °C according to an equation (2).

$$TiH_2 \rightarrow Ti + H_2\uparrow \quad \cdots \quad (2)$$

Presumably, the metallic Ti rapidly reacted with TiO_2 to form Ti_2O_3 at 550 °C. In separate experiments, we performed the reduction of TiO_2 with H_2 or commercial Ti powder at 600 °C (Figure S2). When H_2 was used as a reductant instead of TiH_2, no reduction of TiO_2 occurred. When the commercial metallic Ti powder was used, TiO_2 and metallic Ti remained in the product. Since, generally, metallic Ti is passivated by surface oxide film and removal of the film requires high temperature above 900 °C, the reduction of TiO_2 with the commercial metallic Ti did not proceed at 600 °C. In fact, once the oxide film is removed at high temperature, metallic Ti reduces

TiO_2 to give titanium suboxides immediately.[28,29] From these results, it is supposed that the *in-situ* formed metallic Ti from TiH_2 reacted with TiO_2 according to equation (3).

$$Ti + (2n-1)TiO_2 \rightarrow 2Ti_nO_{2n-1} \quad \cdots(3)$$

For obtaining a titanium suboxide by the present method with TiH_2, an excess amount of TiH_2 over the stoichiometry in the equation (3) was needed. For example, nearly single-phase Ti_2O_3 was obtained from the precursor with $TiO_2/TiH_2 = 2$, though the stoichiometry was $TiO_2/TiH_2 = 3$ according to equation (3). It was probably because water, which was generated by the condensation of OH groups on TiO_2 and was derived from adsorption water, oxidized the metallic Ti and consequently a part of the metallic Ti was consumed according to equation (4).

$$Ti + xH_2O \rightarrow TiO_x + xH_2\uparrow \quad \cdots(4)$$

As mentioned in the introductory part, the conventional methods using metals or metal hydrides other than Ti or TiH_2 inevitably give the metal oxides as by-products coexisting in the product. In contrast, because both TiO_2 and TiH_2 are raw materials for titanium suboxides and H_2 is the only by-product, the present synthesis method has a great advantage over the conventional ones in unnecessity of post-synthesis purification and high atom efficiency.

Compared to Ti_2O_3-com, Ti_2O_3-TH550 showed broad XRD lines with low intensity, suggesting that the crystallite size of Ti_2O_3-TH550 was much smaller than that of Ti_2O_3-com (Figure 1b). In fact, Ti_2O_3-TH550 had uniform spherical nanoparticles with the diameter of around 70 nm observed by SEM (Figure 2a), while Ti_2O_3-com was composed of huge rocky particles with ~100 μm in size (Figure 2b). The spherical nanoparticles of Ti_2O_3-TH550 were also confirmed by

TEM (Figure 3a). There was an ordered fringe pattern on a high magnification image for Ti_2O_3-TH550 (Figure 3b), indicating the high crystallinity. The distance between the fringes was 0.372 nm, which was in accordance with the $d_{(012)}$ spacing of the rhombohedral Ti_2O_3 crystal (0.373 nm). Notably, specific surface area of Ti_2O_3-TH550 (21 m^2 g^{-1}) was much larger than that of Ti_2O_3-com (< 0.1 m^2 g^{-1}) due to nanoparticles (Table 1, and adsorption isotherms are shown in Figure S3).

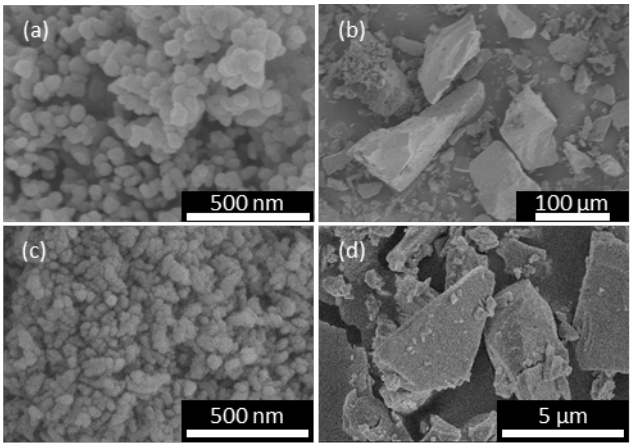

Figure 2. SEM images of (a) Ti_2O_3-TH550, (b) Ti_2O_3-com, (c) TiO_2, and (d) TiH_2.

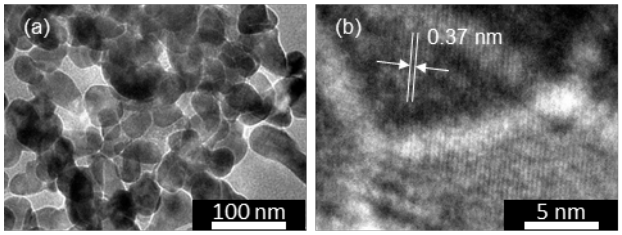

Figure 3. TEM images of Ti_2O_3-TH550 at (a) low and (b) high magnifications.

A TG-DTA profile of Ti_2O_3-TH550 in air is provided in Figure 4. A slight weight loss was observed below 200 °C probably due to desorption of physisorbed water. Then, a significant weight

gain was observed in the temperature range of 200 – 800 °C. Finally, the weight became nearly constant at ~1000 °C. A separate experiment demonstrated that Ti_2O_3-TH550 was completely oxidized to rutile TiO_2 by heating in air at 1000 °C for 1 h (Figure S4). Hence, it is reasonable that the weight gain of Ti_2O_3-TH550 in the TG profile was attributed to oxygen uptake due to the oxidation of Ti_2O_3-TH550. From the amount of oxygen uptake, we estimated the average valence of titanium (Ti_{total}) for Ti_2O_3-TH550 to be 3.08 (Table 1), which was well consistent with that expected from its crystalline phase. Since there was no residual raw material nor by-product detectable by XRD and SEM, the average valence of ~3 for Ti_2O_3-TH550 undoubtedly originated from Ti^{3+} in Ti_2O_3 crystal. From these results, we concluded that the solid-phase reaction of TiO_2 with TiH_2 achieved the synthesis of Ti_2O_3 nanoparticles having a high surface area.

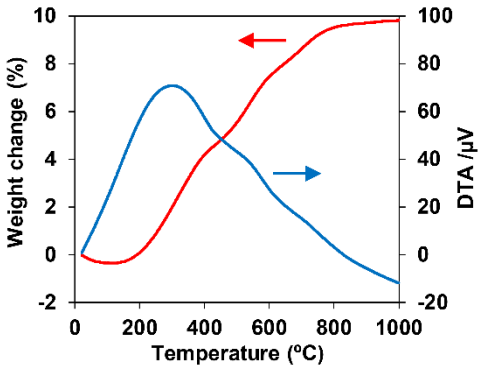

Figure 4. TG-DTA profile of Ti_2O_3-TH550 measured in air.

Phase-controllable synthesis of various titanium suboxides

An advantage of the present synthesis method using TiH_2 is to give various titanium suboxides other than Ti_2O_3 by simply changing TiO_2/TiH_2 ratio (Figure 5). When the precursor

with TiO_2/TiH_2 = 2.75 was heated at 600 °C for 24 h, γ-Ti_3O_5 (JCPDS#40-806) was predominantly formed with a small amount of Ti_2O_3. Heating the precursor with TiO_2/TiH_2 = 3 at 600 °C for 48 h gave Ti_4O_7, whose XRD pattern was in good agreement with the standard one (JCPDS#50-787). Furthermore, Ti_8O_{15} (JCPDS#50-790) was obtained from the precursor with TiO_2/TiH_2 = 5 (Figure 5, Table 1).

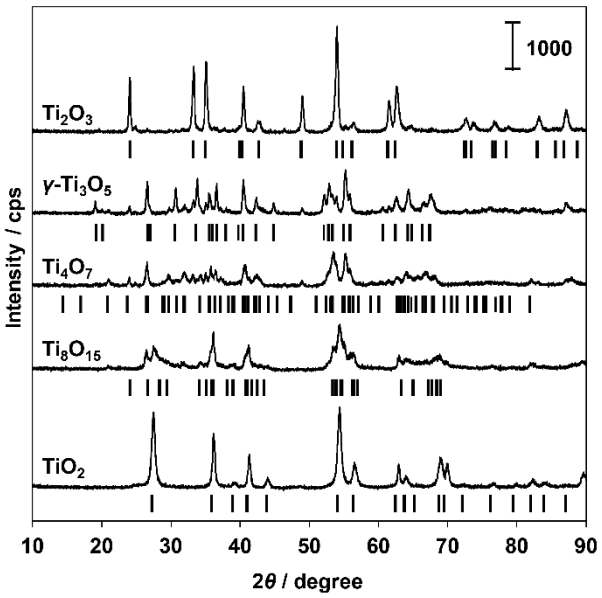

Figure 5. XRD patterns of titanium suboxides of various crystal phases synthesized from TiO_2-TiH_2 mixed precursors. Synthesis conditions are shown in Table 1. Ti_2O_3 synthesized at 600 °C is shown.

Obviously, crystal phase in a product can be controlled by tuning the TiO_2/TiH_2 molar ratio in the precursor. Notably, these titanium suboxide materials were synthesized at 600 °C or lower, resulting in the formation of nanoparticles and large specific surface area about 20 $m^2\ g^{-1}$. For these titanium suboxide samples, Ti_{total} values were in good agreement with those of the main

crystal phases. Thus, various titanium suboxide nanoparticles with different crystal phases can be synthesized, indicating a wide scope of availability for the present synthesis method.

Table 1. Synthesis conditions, specific surface area, and average valence of titanium of various titanium oxides.

Sample	Synthesis conditions			S_{BET} [a] /m^2 g^{-1}	Ti_{total} [b]	Ti_{XRD} [c]
	TiO_2 /TiH_2	Temperature /°C	Time /h			
Ti_2O_3-TH550	2	550	30	21	3.08	3.00
Ti_2O_3-TH600	2	600	24	14	3.00	3.00
Ti_2O_3-TH700	2	700	24	10	2.95	3.00
Ti_2O_3-com	-	-	-	＜0.1	2.93	3.00
γ-Ti_3O_5	2.75	600	24	21	3.26	3.33
Ti_4O_7	3	600	48	19	3.43	3.50
Ti_8O_{15}	5	600	72	16	3.66	3.75
TiO_2	-	-	-	107	4.00	4.00
TiH_2	-	-	-	3	2.08	2.00

[a] Specific surface area calculated by BET method. [b, c] Average valence of total titanium estimated from TG-DTA analysis and from crystal phase observed in XRD, respectively.

Ti species on the surface of TiO_2 and Ti_2O_3

Ti_2O_3-TH550 and Ti_2O_3-TH700 were examined by XPS and compared with rutile TiO_2, which was calcined in air at 550 °C for 5 h and is designated as TiO_2-cal550 (Figure 6). All the spectra had two peaks of Ti $2p_{3/2}$ and $2p_{1/2}$ at 458 and 463 eV, respectively. To discuss the results quantitatively, the peaks of Ti $2p_{3/2}$ whose intensities were higher than those of Ti $2p_{1/2}$ were deconvoluted to two peaks of Ti^{3+} and Ti^{4+} at 455.5 and 457.5 eV, respectively.[64,65] Integrated area

of the deconvoluted peaks and average valence of surface Ti ($Ti_{surface}$), which is defined as (3 × peak area fraction of Ti^{3+} + 4 × peak area fraction of Ti^{4+}), are summarized in Table 2.

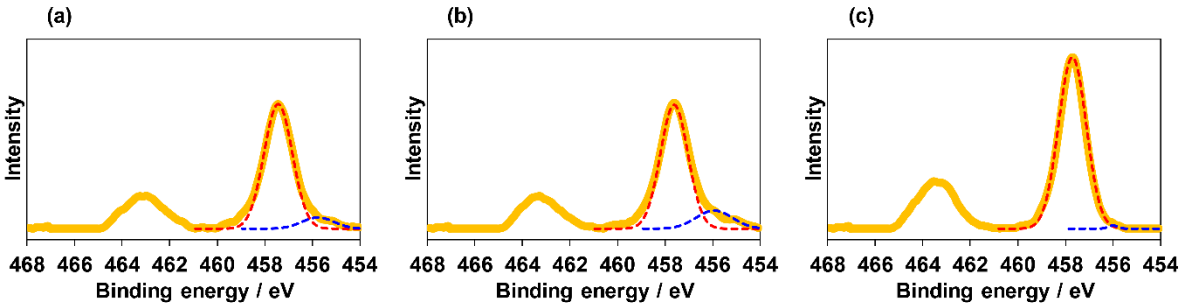

Figure 6. Ti 2p X-ray photoelectron spectra of (a) Ti_2O_3-TH550, (b) Ti_2O_3-TH700, and (c) TiO_2-cal550. Yellow solid line, measured spectra; blue and red dotted lines, deconvoluted peaks of Ti^{3+} and Ti^{4+}, respectively.

Table 2. Abundance of surface Ti species distribution and acid properties for TiO_2 and Ti_2O_3.

Sample	Surface Ti species (%) [a]		$Ti_{surface}$ [b]	Ti_{total} [c]	Acid site [d] /μmol g^{-1}
	Ti^{4+}	Ti^{3+}			
Ti_2O_3-TH550	91	9	3.90	3.08	29
Ti_2O_3-TH700	84	16	3.83	2.95	17
TiO_2-cal550	> 99	< 1	3.99	4.00	45

[a] Calculated from deconvolution of Ti $2p_{3/2}$ XP spectrum. [b] Average valence of surface titanium estimated from Ti $2p_{3/2}$ XP spectrum.

[c] Average valence of total titanium estimated from TG-DTA analysis. [d] Estimated from NH_3-TPD.

For both Ti_2O_3-TH550 and -TH700, the peaks of Ti $2p_{3/2}$ were composed of mainly those of Ti^{4+} and the peaks of Ti^{3+} were small, giving $Ti_{surface}$ around 3.85, though their Ti_{total} were ~3.0. The higher $Ti_{surface}$ than Ti_{total} suggests that Ti^{3+} species on the surface of Ti_2O_3 are labile and

oxidized to Ti^{4+} by the exposure to ambient air. The Ti $2p_{3/2}$ peak for TiO_2-cal550 was predominantly composed of Ti^{4+} and thus, its $Ti_{surface}$ was almost 4.0.

Catalytic properties of Ti_2O_3 and TiO_2 for reaction of furfural with 2-propanol

Catalytic properties of Ti_2O_3 and TiO_2 were investigated in transformation of furfural with 2-propanol (Table 3). There are two reaction pathways; one is acetalization of furfural with generation of water and the other is transfer hydrogenation of furfural to furfuryl alcohol with formation of acetone (Scheme 1).

Table 3. Catalytic performance of titanium oxides and other solid acids for reaction of furfural with 2-propanol.

Entry	Catalyst	S_{BET} /m^2 g^{-1}	Formation rate /mmol h^{-1} g^{-1}	
			Acetal	Alcohol
1	Ti_2O_3-TH550	21	1.6	0.0
2	Ti_2O_3-TH700	10	2.1	0.0
3	Ti_2O_3-com	< 0.1	0.2	0.0
4 [a, b]	TiO_2-cal550	53	0.0	0.2
5 [b]	Zeolite beta	602	1.8	0.0
6 [b]	ZrO_2	76	0.0	2.5
7	Blank	-	0.0	0.0

Reaction conditions: catalyst, 25 mg; furfural, 0.5 mmol; 2-propanol, 2.5 mL; temperature, 90 °C; time, 2 h. [a] Catalyst, 100 mg. [b] Catalyst was calcined in air at 550 °C for 5 h before reaction.

Ti_2O_3-TH550 and Ti_2O_3-TH700 selectively promoted the acetalization of furfural and

gave the formation rate of 1.6 and 2.1 mmol h^{-1} g^{-1}, respectively. Both of the catalysts showed one order of magnitude higher catalytic activity than Ti_2O_3-com (0.2 mmol g^{-1}) due to the high surface area of Ti_2O_3-TH samples, which clearly demonstrated the advantage of the present synthesis method over the conventional one. Furthermore, Ti_2O_3-TH700 showed even higher catalytic activity than zeolite beta, which has been reported to be highly active for the acetalization of furfural.[55]

In contrast to these Ti_2O_3 samples, TiO_2-cal550 did not show any catalytic activity for the acetalization, while it selectively promoted the transfer hydrogenation of furfural at a low reaction rate (0.2 mmol g^{-1}). ZrO_2 selectively promoted the transfer hydrogenation of furfural as well at a higher reaction rate. The different product selectivities between Ti_2O_3 and TiO_2 suggests that the two titanium oxides have different acid properties.

Acid properties of Ti_2O_3 and TiO_2

Acid properties of Ti_2O_3-TH550, Ti_2O_3-TH700, and TiO_2-cal550 were examined by NH_3-TPD (Figure S5) and the number of acid sites estimated is shown in Table 2. These three samples showed broad desorption peaks in the temperature range of 100 – 500 °C with almost the same peak top temperature (320 °C). The number of acid sites on Ti_2O_3-TH550, Ti_2O_3-TH700, and TiO_2-cal550 were 29, 17, and 45 μmol g^{-1}, respectively. It is known that when the number of acid sites with a particular strength is increased, desorption of ammonia is observed at higher temperature due to re-adsorption of ammonia.[66] Ti_2O_3-TH700 with a smaller number of acid sites

gave a desorption peak at a temperature similar to those for Ti_2O_3-TH550 and TiO_2-cal550. Taking the above point into account, it is presumable that Ti_2O_3-TH700 had the stronger acid sites than those on Ti_2O_3-TH550 and TiO_2-cal550. It seems that Ti_2O_3-TH700 showed higher catalytic activity than Ti_2O_3-TH550 for the acetalization due to such stronger acid properties.

It has been reported that zeolite beta and ZrO_2 acted as Brønsted and Lewis acid sites, respectively and promote acetalization and transfer hydrogenation of furfural, respectively.[55,62,63] As shown in the preceding section, Ti_2O_3 selectively promoted the acetalization, while TiO_2 did the transfer hydrogenation. Thus, it is supposed that there is a difference in the types of acid sites between Ti_2O_3 and TiO_2. To confirm this, we measured IR spectra of pyridine adsorbed on them.[67] However, unfortunately, no clear IR band assignable to pyridine was detected for Ti_2O_3, probably because Ti_2O_3 in black color absorbed incident IR almost completely, making absorption bands of pyridine ambiguous.

To examine the relationship between the acid properties and product selectivities for Ti_2O_3 and TiO_2, the reaction of furfural with 2-propanol was conducted in the presence of pyridine and 2,6-lutidine (Figure 7). Although the reaction tests shown in Table 3 were conducted using quite large amount of 2-propanol as a solvent and a reactant, the amount of 2-propanol was decreased and toluene was used as a solvent instead because quite a large amount of 2-propanol could interfere the adsorption of pyridine and 2,6-lutidine on acid sites.

As the amount of pyridine was increased, the activity of Ti_2O_3-TH700 was drastically decreased and eventually it became inactive for the formation of the acetal (Figure 7a). TiO_2-cal550

was also deactivated gradually for the transfer hydrogenation with increase in the amount of pyridine added. The addition of 2,6-lutidine more severely deactivated Ti_2O_3-TH700 than that of pyridine (Figure 7b), because 2,6-lutidine is a base stronger than pyridine.[68] On the other hand, 2,6-lutidine was less effective and hardly deactivated TiO_2-cal550. Similar experiments were conducted using zeolite beta and ZrO_2 (Figure S6). Zeolite beta was completely deactivated by the addition of either pyridine or 2,6-lutidine, similarly to Ti_2O_3-TH700. In contrast, ZrO_2 was still highly active for the transfer hydrogenation in the presence of 2,6-lutidine, similarly to TiO_2-cal550.

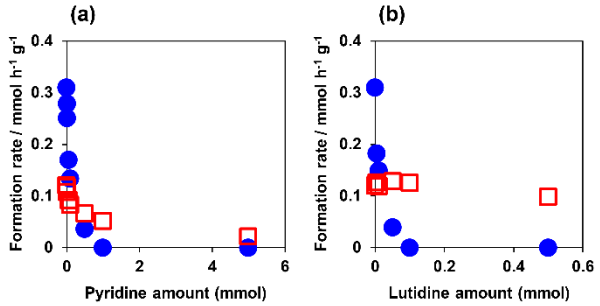

Figure 7. Catalytic activity of Ti_2O_3-TH700 (blue circle) and TiO_2-cal550 (red square) for acetalization and transfer hydrogenation of furfural, respectively in the presence of (a) pyridine or (b) 2,6-lutidine.

Reaction conditions: catalyst, Ti_2O_3 25 mg or TiO_2 100 mg; furfural, 0.5 mmol; 2-propanol, 5 mmol; toluene, 2.5 mL; pyridine, 0 – 5 mmol or lutidine, 0 – 0.5 mmol; temperature, 90 °C; time, 3 h.

Generally, pyridine can adsorb on both Brønsted and Lewis acid sites, while 2,6-lutidine

can adsorb on only Brønsted acid sites since the two methyl groups sterically hinder the nitrogen atom from approaching a metal center of Lewis acid site.[69] Considering the same product selectivity as zeolite beta and the deactivation behavior by adding either pyridine or 2,6-lutidine, Ti_2O_3-TH700 behaved as a catalyst with Brønsted acid sites. Meanwhile, TiO_2-cal550 behaved as a Lewis acid catalyst likewise ZrO_2. Recently, it is reported that tin oxide supported on silica reacts with 2-propanol to form acidic OH groups, which catalytically act as Brønsted acid sites.[70] Although it is still unclear whether Ti_2O_3-TH700 had Brønsted acid sites originally or formed acidic OH groups *in situ* by the reaction with 2-propanol, the different product selectivities between Ti_2O_3 and TiO_2 is probably due to the difference in the types of catalytically active acid sites.

Involvement of Ti^{3+} in catalysis for acetalization of furfural

Ti_2O_3-TH700 showed a little faster rate for the formation of acetal than Ti_2O_3-TH550 despite the smaller specific surface area (Table 3). In addition, TiO_2-cal550, which was poor of Ti^{3+}, showed no activity for the acetalization. These results indicated that Ti^{3+} on the surface of Ti_2O_3 was involved in the formation of Brønsted acid sites to promote the acetalization and that Ti_2O_3-TH700 showed higher catalytic activity than Ti_2O_3-TH550 due to the higher abundance of Ti^{3+} on the surface.

A relationship between the abundance of Ti^{3+} and the catalytic activity for the acetalization was investigated using several titanium oxide samples obtained by calcination of Ti_2O_3-TH700 at different temperatures (Figure 8). The abundance of Ti^{3+} on the surface of Ti_2O_3-TH700 was

steeply decreased by the calcination at 100 °C and then little by little decreased by increasing the temperature up to 800 °C (Figures 8a and S7). The bulk structure of Ti_2O_3 was still intact after the calcination at 200 °C (Figure S8) and Ti_{total} was only slightly increased from 2.95 to 3.02, indicating that oxidation of Ti^{3+} occurred mainly on the surface at 200 °C or lower. However, the diffraction lines of rutile TiO_2 appeared with the calcination at 400 °C and finally, rutile TiO_2 became the predominant phase at 700 °C. The specific surface area of Ti_2O_3-TH700 did not change even after the calcination at 700 °C.

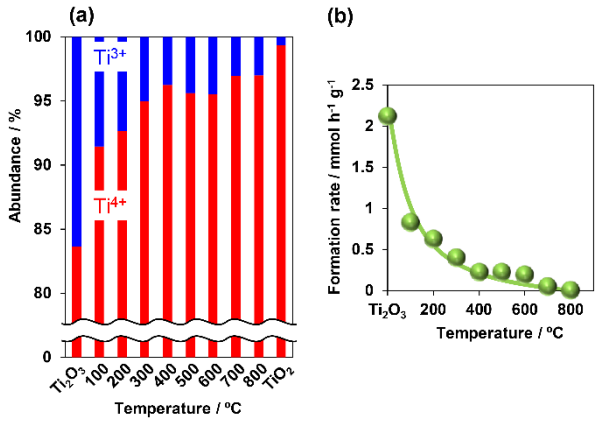

Figure 8. (a) Abundance of surface Ti species and (b) catalytic activity of Ti_2O_3-TH700 calcined in air at different temperatures for acetalization of furfural. Ti_2O_3-TH700 was calcined in air at 100 – 800 °C for 0.5 h. Reaction conditions were the same as those for Table 3.

The catalytic activity for the acetalization was drastically decreased by the calcination at 100 °C and then gradually decreased along with the calcination temperature (Figure 8b). The calcination at 700 °C or higher gave titanium oxides of mainly rutile phase, being almost inactive

for the acetalization. There is a clear correlation between the abundance of Ti^{3+} and the catalytic activity for the acetalization. Considering that the bulk structure and specific surface area were retained after the calcination up to 400 °C, it is reasonable to suppose that Ti_2O_3-TH700 was deactivated due to the oxidation of the surface Ti^{3+} to Ti^{4+}. These results clearly demonstrated that Ti^{3+} on the surface of Ti_2O_3 was involved in the formation of Brønsted acid sites to promote the acetalization.

After the calcination at 700 °C or higher, Ti^{3+} still slightly remained on the samples. However, these samples showed no activity for the acetalization, implying that not all but specific Ti^{3+} are active for the acetalization. The differences in acid strength and catalytic activity between Ti_2O_3-TH550 and Ti_2O_3-TH700 might be related to population distributions of active Ti^{3+} species on these samples. It is interesting to note that Ti^{4+} generated on the surface of Ti_2O_3 by the air exposure and the calcination showed no activity for the transfer hydrogenation of furfural. Therefore, it is considered that a specific Ti^{4+} on the surface of TiO_2 is active for the transfer hydrogenation and that other types of inactive Ti^{4+} were generated on Ti_2O_3.

Conclusions

Magneli-phase titanium suboxide nanoparticles were synthesized through solid-phase reaction of TiO_2 with TiH_2 under vacuum. The crystal phase in a product can be controlled by simply tuning the TiO_2/TiH_2 molar ratio in a precursor and a series of titanium suboxides including Ti_2O_3, γ-Ti_3O_5, Ti_4O_7 and Ti_8O_{15} were successfully synthesized. Ti_2O_3 with a particle size of ~70

nm was obtained by heating a mixture with TiO_2/TiH_2 = 2 at 550 °C for 30 h. Specific surface area of Ti_2O_3 was 21 $m^2\ g^{-1}$, which was much larger than that of the commercial one (< 0.1 $m^2\ g^{-1}$).

Ti^{3+} species on the surface of Ti_2O_3 are labile and mostly oxidized to Ti^{4+} only by the exposure to ambient air. In the reaction of furfural with 2-propanol, Ti_2O_3 selectively promoted the acetalization of furfural, while TiO_2 promoted the transfer hydrogenation of furfural. Ti_2O_3 showed the high catalytic activity for the acetalization, comparable to zeolite beta. Ti^{3+} on the surface of Ti_2O_3 formed catalytically active sites for the acetalization.

Supporting Information

Additional data on characterization and catalytic reactions is provided as Supporting Information.

Author contribution

M. N. conducted all the experiments. S. M. and J. H. conducted preliminary experiments. R. O. and Y. K. managed this study and prepared the manuscript. All authors have approved the final version of the manuscript.

Conflicts of interest

There are no conflicts of interest to declare.

Acknowledgement

This work was supported by Iketani Science and Technology Foundation. The analyses of TEM and XPS were conducted with the instruments at the Institute for Catalysis, Hokkaido University.

References

[1] Clarke, F. W.; Washington, H. S. The Composition of the Earth's Crust. *United States Geological Survey Professional Paper*. **1924**, 127.

[2] Chen, X.; Liu, L.; Huang, F. Black Titanium Dioxide (TiO_2) Nanomaterials. *Chem. Soc. Rev.* **2015**, *44*, 1861-1885.

[3] Xu, B.; Sohn, H. Y.; Mohassab, Y.; Lan, Y. Structures, Preparation and Applications of Titanium Suboxides. *RSC Adv.* **2016**, *6*, 79706-79722.

[4] Andersson, S.; Collen, B.; Kuylenstierna, U.; Magneli, A. Phase Analysis Studies on the Titanium-Oxygen System. *Acta. Chem. Scand.* **1957**, *11*, 1641-1652.

[5] Lakkis, S.; Schlenker, C.; Chakraverty, B. K.; Buder R.; Marezio, M. Metal-Insulator Transitions in Ti_4O_7 Single Crystals: Crystal Characterization, Specific Heat, and Electron Paramagnetic Resonance. *Phys. Rev. B.* **1976**, *14*, 1429-1440.

[6] Kolbrecka, K.; Przyluski, J. Sub-Stoichiometric Titanium Oxides as Ceramic Electrodes for Oxygen Evolution-Structural Aspects of the Voltammetric Behaviour of Ti_nO_{2n-1}. *Electrochim. Acta*. **1994**, *39*, 1591-1595.

[7] Bowden, M. E.; White, G. V.; Brown, I. W. M.; Ryan, M. J.; Gainsford, G. J. Improved Powder Diffraction Patterns for the Titanium Suboxides Ti_nO_{2n-1} ($4 \leq n \leq 9$). *Powder Diffr.* **1996**, *11*,

60-68.

[8] Ioroi, T.; Siroma, Z.; Fujiwara, N.; Yamazaki, S.; Yasuda, K. Sub-Stoichiometric Titanium Oxide-Supported Platinum Electrocatalyst for Polymer Electrolyte Fuel Cells. *Electrochem. Commun.* **2005**, *7*, 183-188.

[9] Radecka, M.; Trenczek-Zajac, A.; Zakrzewska, K.; Rekas, M. Effect of Oxygen Nonstoichiometry on Photo-Electrochemical Properties of TiO_{2-x}. *J. Power Sources*. **2007**, *173*, 816-821.

[10] Siracusano, S.; Baglio, V.; D'Urso, C.; Antonucci, V.; Arico, A. S. Preparation and Chatacterization of Titanium Suboxides as Conductive Supports of IrO_2 Electrocatalysts for Application in SPE Electrocatalysers. *Electrochim. Acta*. **2009**, *54*, 6292-6299.

[11] Martyanov, I. N.; Berger, T.; Diwald, O.; Rodrigues, S.; Klabunde, K. J. Enhancement of TiO_2 Visible Light Photoactivity Through Accumulation of Defects During Reduction-Oxidation Treatment. *J. Photoch. Photobio. A.* **2010**, *212*, 135-141.

[12] Li, X.; Zhu, A. L.; Qu, W.; Wang, H.; Hui, R.; Zhang, L.; Zhang, J. Magneli Phase Ti_4O_7 Electrode for Oxygen Reduction Reaction and Its Implication for Zinc-Air Rechargeable Batteries. *Electrochim. Acta*. **2010**, *55*, 5891-5898.

[13] Yao, C.; Li, F.; Li, X.; Xia, D. Fiber-Like Nanostructured Ti_4O_7 Used as Durable Fuel Cell Catalyst Support in Oxygen Reduction Catalysis. *J. Mater. Chem.* **2012**, *22*, 16560-16565.

[14] Tanaka, K.; Nasu, T.; Miyamoto, Y.; Ozaki, N.; Tanaka, S.; Nagata, T.; Hakoe, F.; Yoshikiyo, M.; Nakagawa, K.; Umeta, Y.; Imoto, K.; Tokoro, H.; Namai, A.; Ohkoshi, S. Structural Phase

Transition between γ-Ti_3O_5 and δ-Ti_3O_5 by Breaking of a One-Dimensionally Conducting Pathway. *Cryst. Growth Des.* **2015**, *15*, 653-657.

[15] Geng, P.; Su, J.; Miles, C.; comninellis, C.; Chen, G. Highly-Ordered Magneli Ti_4O_7 Nanotube Arrays as Effective Anodic Material for Electro-Oxidation. *Electrochim. Acta*. **2015**, *153*, 316-324.

[16] Won, J.-E.; Kwak, D.-H.; Han, S.-B.; Park, H.-S.; Park, J.-Y.; Ma, K.-B.; Kim, D.-H.; Park, K.-W. PtIr/Ti_4O_7 as a Bifunctional Electrocatalyst for Improved Oxygen Reduction and Oxygen Evolution Reactions. *J. Catal.* **2018**, *358*, 287-294.

[17] Fan, Y.; Feng, X.; Zhou, W.; Murakami, S.; Kikuchi, K.; Nomura, N.; Wang, L.; Jiang, W.; Kawasaki, A. Preparation of Monophasic Titanium Sub-Oxides of Magneli Phase with Enhanced Thermoelectric Performance. *J. Eur. Ceram. Soc.* **2018**, *38*, 507-513.

[18] Koc, R.; Folmer, J. S. Carbothermal Synthesis of Titanium Carbide Using Ultrafine Titania Powders. *J. Mater. Sci.* **1997**, *32*, 3101-3111.

[19] Afir, A.; Achour, M.; Saoula, N. X-ray Diffraction Study of Ti-O-C System at High Temperature and In a Continuous Vacuum. *J. Alloy Compd.* **1999**, *288*, 124-140.

[20] Lefort, P.; Maitre, A.; Tristant, P. Influence of the Grain Size on the Reactivity of TiO_2/C Mixtures. *J. Alloy Compd.* **2000**, *302*, 287-298.

[21] Dewan, M. A. R.; Zhang, G.; Ostrovski, O. Carbothermal Reduction of Titania in Different Gas Atmospheres. *Metal. Mater. Trans. B*. **2009**, *40B*, 62-69.

[22] Adamaki, V.; Clemens, F.; Ragulis, P.; Pennock, S. R.; Taylor, J.; Bowen, C. R. Manufacturing

and Characterization of Magneli Phase Conductive Fibres. *J. Mater. Chem. A.* **2014**, *2*, 8328-8333.

[23] Chai, G.; Huang, W.; Shi, Q.; Zheng, S.; Wei, D. Preparation and Characterization of λ-Ti_3O_5 by Carbothermal Reduction of TiO_2. *J. Alloy Compd.* **2015**, *621*, 404-410.

[24] Wang, L.; Zhang, X.; Liu, W.; Xu, W.; Singh, A.; Lin, Y. Electrochemical Properties of Ti_3O_5 Powders Prepared by Carbothermal Reduction. *J. Mater. Sci.–Mater. El.* **2017**, *28*, 6421-6425.

[25] Liu, K.; Wang, Y.; Di, Y.; Peng, J.; You, J.; Feng, N.; Zhang, Y. Preparation of Porous Ti_2O_3 via a Carbothermal Reduction of Titanium Dioxide. *Ceram. Int.* **2018**, *44*, 1007-1012.

[26] Mao, X.; Yuan, F.; Zhou, A.; Jing, W. Magneli Phases Ti_nO_{2n-1} as Novel Ozonation Catalysts for Effective Mineralization of Phenol. *Chinese J. Chem. Eng.* **2018**, *26*, 1978-1984.

[27] Hauf, C.; Kneip, R.; Pfaff, G. Preparation of Various Titanium Suboxide Powders by Reduction of TiO_2 with Silicon. *J. Mater. Sci.* **1999**, *34*, 1287-1292.

[28] Acha, C.; Monteverde, M.; Nunez-Reguiero, M.; Kuhn, A.; Franco, M. A. A. Electrical Resistivity of the Ti_4O_7 Magneli Phase under High Pressure. *Eur. Phys. J. B.* **2003**, *34*, 421-428.

[29] Gusev, A. A.; Avvakumov, E. G.; Vinokurova, O. B. Synthesis of Ti_4O_7 Magneli Phase Using Mechanical Activation. *Sci. Sinter.* **2003**, *35*, 141-145.

[30] Kitada, A.; Hasegawa, G.; Kobayashi, Y.; Kanamori, K.; Nakanishi, K.; Kageyama, H. Selective Preparation of Macroporous Monoliths of Conductive Titanium oxides Ti_nO_{2n-1} (n = 2, 3, 4, 6). *J. Am. Chem. Soc.* **2012**, *134*, 10894-10898.

[31] He, C.; Chang, S.; Huang, X.; Wang, Q.; Mei, A.; Shen, P. K. Direct Synthesis of Pure Single-Crystalline Magneli Phase Ti_8O_{15} Nanowires as Conductive Carbon-Free Materials for Electrocatalysis. *Nanoscale*. **2015**, *7*, 2856-2861.

[32] Tominaka, S.; Tsujimoto, Y.; Matsushita, Y.; Yamaura, K. Synthesis of Nanostructured Reduced Titanium Oxide: Crystal Structure Transformation Maintaining Nanomorphology. *Angew. Chem. Int. Ed.* **2011**, *50*, 7418-7421.

[33] Kitada, A.; Hasegawa, G.; Kobayashi, Y.; Miyazaki, K.; Abe, T.; Kanamori, K.; Nakanishi, K.; Kageyama, H. Hierarchically Porous Monoliths of Oxygen-Deficient Anatase TiO_{2-x} with Electronic Conductivity. *RSC Adv.* **2013**, *3*, 7205-7208.

[34] Wang, S.; Yang, X.; Wang, Y.; Liu, L.; Guo, Y.; Guo, H. Morphology-Controlled Synthesis of Ti^{3+} Self-Doped Yolk-Shell Structure Titanium Oxide with Superior Photocatalytic Activity under Visible Light. *J. Solid State Chem.* **2014**, *213*, 98-103.

[35] Tsujimoto, Y.; Matsushita, Y.; Yu, S.; Yamaura, K.; Uchikoshi, T. Size Dependence of Structural, Magnetic, and Electrical Properties in Corundum-Type Ti_2O_3 Nanoparticles Showing Insulator-Metal Transition. *J. Asian Ceram. Soc.* **2015**, *3*, 325-333.

[36] Tsujimoto, Y. Low-Temperature Solid-State Reduction Approach to Highly Reduced Titanium Oxide Nanocrystals. *J. Ceram. Soc. Jpn.* **2018**, *126*, 609-613.

[37] Sinhamahapatra, A.; Lee, H.-Y.; Shen, S.; Mao, S. S.; Yu, J.-S. H-doped TiO_{2-x} Prepared with MgH_2 for Highly Efficient Solar-Driven Hydrogen Production. *Appl. Catal. B-Environ.* **2018**, *237*, 613-621.

[38] Toyoda, M.; Yano, T.; Tryba, B.; Mozia, S.; Tsumura, T.; Inagaki, M. Preparation of Carbon-Coated Magneli Phases Ti_nO_{2n-1} and Their Photocatalytic Activity Under Visible Light. *Appl. Catal. B-Environ.* **2009**, *88*, 160-164.

[39] Portehault, D.; Maneeratana, V.; Candolfi, C.; Veremchuk, I.; Grin, Y.; Sanchez, C.; Antonietti, M. Facile General Route Toward Tunable Magneli Nanostructures and Their Use as Thermoelectric Metal Oxide/Carbon Nanocomposites. *ACS Nano*. **2011**, *5*, 9052-9061.

[40] Regonini, D.; Dent, A. C. E.; Bowen, C. R.; Pennock, S. R.; Taylor, J. Impedance Spectroscopy Analysis of Ti_nO_{2n-1} Magneli Phases. *Mater. Lett.* **2011**, *65*, 3590-3592.

[41] Takeuchi, T.; Fukushima, J.; Hayashi, Y.; Takizawa, H. Synthesis of Ti_4O_7 Nanoparticles by Carbothermal Reduction Using Microwave Rapid Heating. *Catalysts*. **2017**, *7*, 65.

[42] Tanaka, T.; Kumagai, H.; Hattori, H.; Kudo, M.; Hasegawa, S. Generation of Basic Sites on TiO_2 by Reduction with H_2. *J. Catal.* **1991**, *127*, 221-226.

[43] Liu, G.; Rodriguez, J. A.; Hrbek, J.; Long, B. T.; Chen, D. A. Interaction of Thiophene with Stoichiometric and Reduced Rutile TiO_2(1 1 0) Surfaces: Role of Ti^{3+} Sites in Desulfurization Activity. *J. Mol. Catal. A-Chem.* **2003**, *202*, 215-227.

[44] Barzan, C.; Groppo, E.; Bordiga, S.; Zecchina, A. Defect Sites in H_2-Reduced TiO_2 Convert Ethylene to High Density Polyethylene without Activator. *ACS Catal.* **2014**, *4*, 986-989.

[45] Zeng, L.; Song, W.; Li, M.; Zeng, D.; Xie, C. Catalytic Oxidation of Formaldehyde on Surface of H-TiO_2/H-C-TiO_2 without Light Illumination at Room Temperature. *Appl. Catal. B-Environ.* **2014**, *147*, 490-498.

[46] Clark, P. D.; Dowling, N. I.; Huang, M. Role of Ti^{3+} in CS_2 Conversion Over TiO_2 Claus Catalyst. *Appl. Catal. A-Gen.* **2015**, *489*, 111-116.

[47] Liu, C.; Zhang, A.-Y.; Pei, D.-N.; Yu, H.-Q. Efficient Electrochemical Reduction of Nitrobenzene by Defect-Engineered TiO_{2-x} Single Crystals. *Environ. Sci. Technol.* **2016**, *50*, 5234-5242.

[48] Ding, Y.; Zhang, X.; Chen, L.; Wang, X.; Zhang, N.; Liu, Y.; Fang, Y. Oxygen Vacancies Enabled Enhancement of Catalytic Property of Al Reduced Anatase TiO_2 in the Decomposition of High Concentration Ozone. *J. Solid State Chem.* **2017**, *250*, 121-127.

[49] He, M.; Ji, J.; Liu, B.; Huang, H. Reduced TiO_2 with Tunable Oxygen Vacancies for Catalytic Oxidation of Formaldehyde at Room Temperature. *Appl. Surf. Sci.* **2019**, *473*, 934-942.

[50] Zeitsch, K.J. The Chemistry and Technology of Furfural and Its Many Byproducts, Sugar Series vol. 13, 1st ed., Elsevier, The Netherlands, 2000.

[51] Corma, A.; Iborra S.; Velty, A. Chemical Routes for the Transformation of Biomass into Chemicals. *Chem. Rev.*, **2007**, *107*, 2411-2502.

[52] Bozell, J. J.; Petersen, G. R. Technology Development for the Production of Biobased Products from Biorefinery Carbohydrates—the US Department of Energy's "Top 10" Revisited. *Green Chem.*, **2010**, *12*, 539-554.

[53] Rosatella, A. A.; Simeonov, S. P.; Frade, R. F. M.; Afonso, C. A. M. 5-Hydroxymethylfurfural (HMF) as a Building Block Platform: Biological Properties, Synthesis and Synthetic Applications. *Green Chem.*, **2011**, *13*, 754–793.

[54] Arias, K. S.; Al-Resayes, S. I.; Climent, M. J.; Corma, A.; Iborra, S. From Biomass to Chemicals: Synthesis of Precursors of Biodegradable Surfactants from 5-Hydroxymethylfurfural. *ChemSusChem*, **2013**, *6*, 123-131.

[55] Rubio-Caballero, J. M.; Saravanamurugan, S.; Maireles-Torres P.; Riisager, A. Acetalization of Furfural with Zeolites Under Benign Reaction Conditions. *Catal. Today*, **2014**, *234*, 233-236.

[56] Kanai, S.; Nagahara, I.; Kita, Y.; Kamata, K.; Hara, M. A Bifunctional Cerium Phosphate Catalyst for Chemoselective Acetalization. *Chem. Sci.*, **2017**, *8*, 3146-3153.

[57] Kim, M.; Su, Y.; Fukuoka, A.; Hensen, E. J. M.; Nakajima, K. Aerobic Oxidation of 5-(Hydroxymethyl)furfural Cyclic Acetal Enables Selective Furan-2,5-Dicarboxylic Acid Formation with CeO_2-Supported Gold Catalyst. *Angew. Chem. Int. Ed.*, **2018**, *57*, 8235-8239.

[58] Lewis, J. D.; Van de Vyver, S.; Crisci, A. J.; Gunther, W. R.; Michaelis, V. K.; Griffin, R. G.; Román-Leshkov Y. A Continuous Flow Strategy for the Coupled Transfer Hydrogenation and Etherification of 5-(Hydroxymethyl)furfural Using Lewis Acid Zeolites. *ChemSusChem*, **2014**, *7*, 2255-2265.

[59] Jae, J.; Mahmoud, E.; Lobo, R. F.; Vlachos, D. G. Cascade of Liquid-Phase Catalytic Transfer Hydrogenation and Etherification of 5-Hydroxymethylfurfural to Potential Biodiesel Components Over Lewis Acid Zeolites. *ChemCatChem*, **2014**, *6*, 508-513.

[60] Koehle, M.; Lobo, R. F. Lewis Acidic Zeolite Beta Catalyst for the Meerwein–Ponndorf–Verley Reduction of Furfural. *Catal. Sci. Technol.*, **2016**, *6*, 3018-3026.

[61] Lanzafame, P.; Papanikolaou, G.; Perathoner, S.; Centi, G.; Migliori, M.; Catizzone, E.; Aloise,

A.; Giordano, G.; Direct Versus Acetalization Routes in the Reaction Network of Catalytic HMF Etherification. *Catal. Sci. Technol.*, **2018**, *8*, 1304-1313.

[62] Komanoya, T.; Nakajima, K.; Kitano, M.; Hara, M. Synergistic Catalysis by Lewis Acid and Base Sites on ZrO_2 for Meerwein−Ponndorf−Verley Reduction. *J. Phys. Chem. C*, **2015**, *119*, 26540-26546.

[63] Gonell, F.; Boronat M.; Corma, A. Structure–Reactivity Relationship in Isolated Zr Sites Present in Zr-Zeolite and ZrO_2 for the Meerwein– Ponndorf–Verley Reaction. *Catal. Sci. Technol.*, **2017**, *7*, 2865-2873.

[64] Kuznetsov, M. V.; Zhuravlev, J. F.; Zhilyaev V. A.; Gubanov, V. A. XPS Study of the Nitrides, Oxides and Oxynitrides of Titanium. *J. Electron Spectrosc.*, **1992**, *58*, 1-9.

[65] Bertoti, I.; Mohai, M.; Sullivan J. L.; Saied, S. O. Surface Characterisation of Plasma-Nitrided Titanium: an XPS Study. *Appl. Surf. Sci.*, **1995**, *84*, 357-371.

[66] Cvetanovic, R. J.; Amenomiya, Y. A Temperature Programmed Desorption Technique for Investigation of Practical Catalysts. *Cataly. Rev.*, **1972**, *6*, 21-48.

[67] Parry, E. P. An Infrared Study of Pyridine Adsorbed on Acidic Solids. Characterization of Surface Acidity. *J. Catal.*, **1963**, *2*, 371-379.

[68] Kaljurand, I.; Kütt, A.; Sooväli, L.; Rodima, T.; Mäemets, V.; Leito, I.; Koppel, I. A. Extension of the Self-Consistent Spectrophotometric Basicity Scale in Acetonitrile to a Full Span of 28 p*K*a Units: Unification of Different Basicity Scales. *J. Org. Chem.* **2005**, *70*, 1019-1028.

[69] Benesi, H. A. Determination of Proton Acidity of Solid Catalysts by Chromatographic

Adsorption of Sterically Hindered Amines. *J. Catal.*, **1973**, *28*, 176-178.

[70] Beletskiy, E. V.; Hou, X.; Shen, Z.; Gallagher, J. R.; Miller, J. T.; Wu, Y.; Li, T.; Kung, M. C.; Kung, H. H. Supported Tetrahedral Oxo-Sn Catalyst: Single Site, Two Modes of Catalysis. *J. Am. Chem. Soc.*, **2016**, *138*, 4294-4297.